Thermal expansion coefficient of WRe alloys from first principles

Thomas Dengg,[1,2] Vsevolod Razumovskiy,[1] Lorenz Romaner,[1] Georg Kresse,[3] Peter Puschnig,[2] and Jürgen Spitaler[1]
[1]*Materials Center Leoben Forschung GmbH, Roseggerstraße 12, 8700 Leoben, Austria*
[2]*University of Graz, Institute of Physics, NAWI Graz, Universitätsplatz 5, 8010 Graz, Austria*
[3]*Institut für Materialphysik and Center for Computational Materials Science, Universität Wien, 1090 Wien, Austria*
(Received 20 December 2016; revised manuscript received 18 April 2017; published 26 July 2017)

We calculate the coefficient of thermal expansion (CTE) in tungsten-rhenium random alloys for Re concentrations between 0% and 50% and for temperatures up to 2400 K by employing the quasiharmonic approximation within the *ab initio* framework of density functional theory. We treat chemical disorder by the virtual crystal approximation and compute the phonon density of states at two levels of sophistication. While the traditional Debye-Grüneisen (DG) model fails to account for the experimentally observed increase in CTE upon Re addition for concentrations above 10% Re, explicit phonon calculations within density functional perturbation theory lead to an overall good agreement with experiment. Thereby we identify the pronounced phonon softening and anisotropy between transversal and longitudinal modes in W-Re to be responsible for the breakdown of the DG model.

DOI: 10.1103/PhysRevB.96.035148

I. INTRODUCTION

In this work we study the effect of alloying on the coefficient of thermal expansion (CTE) in W-Re random alloys. This system has been chosen because Re is an important alloying element in W due to the well-known ductilization effect induced by Re. For instance, it has been shown that Re leads to a softening in shear modulus and alters phonon properties [1], crystal lattice stability [2], as well as the dislocation core structure [3,4] and the grain boundary segregation and cohesion [5]. The effects of Re on the CTE are, however, still poorly understood. Experimentally, the CTE of WRe alloys is characterized by two important and unexpected features [6–8] which we have illustrated in Fig. 1. First, there is an overall increase in the CTE upon Re addition which appears to be unexpected because it is known that the bulk modulus increases with Re addition and the lattice parameter decreases indicative of a stiffening of bonds [9]. Such behavior is, however, generally accompanied by a decrease of the CTE. Second, there is an anomaly in the CTE as a function of Re content around 10% Re. This anomaly can be best seen at low temperature as a nonmonotonic behavior of the CTE exhibiting a local minimum around 12% Re. At 1000 K, only a remnant of this anomaly is present, while at even larger temperatures a monotonous increase of the CTE is found upon addition of Re. Based on this observation, Andrianova *et al.* have attributed the anomaly to short range order effects [7]. However, the role of short range order appears questionable, since more recently it has been shown that the ordering energy in W-Re is in the order of 20 meV only [10]. Hence, WRe alloys are expected to be disordered already at room temperature and therefore cannot be made responsible for the anomaly between 400 and 1000 K. We rather propose that this anomaly can be accounted for by the phonon properties of these alloys. In order to answer the question which physical mechanisms are responsible for (i) the overall increase in the CTE upon Re addition and (ii) the anomaly, we calculate elastic constants, phonon spectra, and mode Grüneisen parameters. Moreover, we present results obtained with the traditional Debye-Grüneisen model [11,12]. Even though this model contains strong simplifications, it is still widely used when it comes to predicting thermal properties in high-throughput studies or complex structures, including random alloys, where explicit phonon calculations are not feasible [13–23]. By using this model we want to assess whether a computationally less expensive approach can also lead to satisfactory results for the studied alloying system.

The paper is organized as follows: In Sec. II we introduce the basic theory of thermal expansion within the quasiharmonic approximation (QHA) and present the approaches to compute the phonon density of states used in this work, namely the Debye-Grüneisen (DG) model and the explicit phonon calculations using density functional perturbation theory (DFPT). Section III presents the computational details for the electronic structure and phonon calculations valid throughout this paper. Section IV is dedicated to the results, including elastic properties, phonons, and thermal expansion.

II. THEORY

To compute the CTE within the QHA, the volume (V) and temperature (T) dependent free energy is considered:

$$F(V,T) = U(V) + F_{\mathrm{vib}}(V,T) + F_{\mathrm{el}}(V,T). \tag{2.1}$$

Here U is the internal energy, F_{vib} is the vibrational, and F_{el} is the electronic part of the free energy. Note that we disregard the electronic free energy since the combined effect of higher order anharmonic, vacancy, and electronic contribution is considered to be small up to 1500 K due to a fortunate error cancellation [24,25]. Thus we also neglect anharmonic contributions beyond the volume dependence of phonon frequencies included in the QHA. We note that the treatment of such anharmonicity effects goes beyond the scope of this work but would be desirable in future assessments of the alloy system to make quantitative predictions of the CTE above 1500 K.

Within the QHA, the vibrational free energy is obtained by integrating the volume dependent phonon density of states

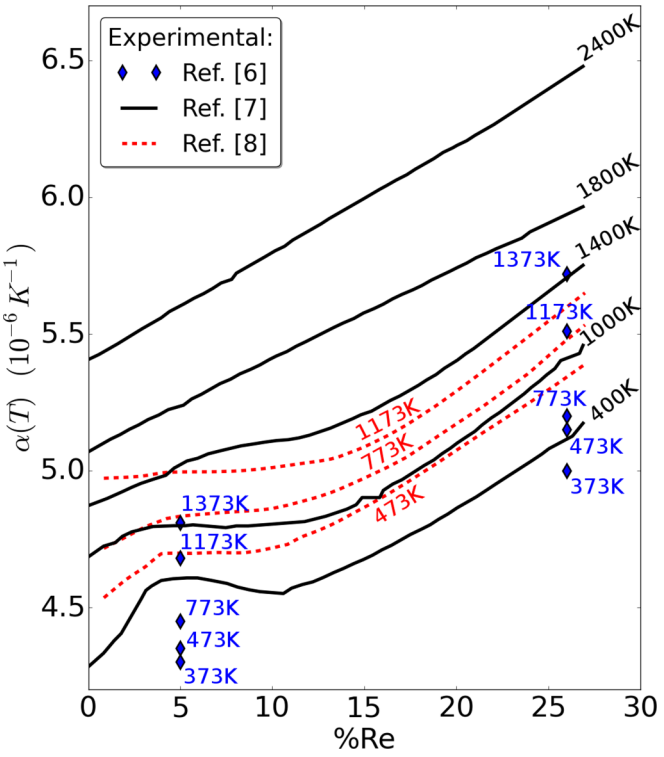

FIG. 1. Experimental measurements of the CTE of WRe alloys as a function or Re concentration. Triangles refer to experiments conducted by Plansee [6], solid and dashed lines to experiments conducted by Andrianova *et al.* [7] and Zaichenko *et al.* [8] respectively.

$D(\epsilon, V)$ over all energy states ϵ [26]:

$$F_{\text{vib}}(V,T) = \int_0^\infty d\epsilon\, D(\epsilon,V) \times \left\{ \frac{\epsilon}{2} + k_B T \ln\left[1 - \exp\left(-\frac{\epsilon}{k_B T}\right)\right]\right\}, \quad (2.2)$$

where k_B is the Boltzmann constant. To get accurate *ab initio* phonon dispersion relations and the resulting phonon density of states, we applied density functional perturbation theory (DFPT) [27–29]. In this method, small perturbations of the atomic positions are used to get an electron density response. By using linear response theory, the dynamical matrix is obtained on a grid of k points in the Brillouin zone. The eigenvalues of the dynamical matrix yield the phonon frequencies $\omega_i(k)$ which are used to obtain the phonon density of states (DOS) by numerically integrating over the Brillouin zone. By computing the phonon DOS $D(\epsilon,V)$ for a set of volumes, the vibrational free energy $F_{\text{vib}}(V,T)$ is obtained from Eq. (2.2).

For the sake of comparison, we also employ the classical Debye-Grüneisen (DG) model as a greatly simplified approach to obtain the phonon DOS. In the Debye model [11,12], the phonon dispersion is simplified by assuming a single, linear dispersion relation for both the longitudinal and the transverse acoustic phonon branches, which leads to a simple parabolic form of the phonon density of states which is cut off at the Debye frequency. The volume-dependent Debye temperature $\Theta_D(V)$ solely depends on the sound velocity, and thus on the slope of the assumed dispersion relation. As a consequence, Θ_D may also be related to the bulk modulus in the following manner [12,30]:

$$\Theta_D(V_0) = \frac{h}{k_B}\left(\frac{3}{4\pi V_0}\right)^{1/3} C \left(\frac{V_0^{1/3} B_0}{M}\right)^{1/2}. \quad (2.3)$$

Here M is the atomic mass, V_0 and B_0 are the equilibrium volume and bulk modulus, respectively, and h is the Planck constant. The factor C is a scaling factor which is, based on experimental data from Ref. [31], set to 0.617 in the traditional DG model as proposed by Moruzzi *et al.* [11]. The volume dependence of $\Theta_D(V)$ arises via a volume dependence of the bulk modulus. Within the Debye-Grüneisen approach, Θ_D is expanded around the equilibrium volume V_0 via the expression

$$\frac{\Theta_D(V)}{\Theta_D(V_0)} = \left(\frac{V_0}{V}\right)^\gamma, \quad (2.4)$$

where γ is the Grüneisen constant. Note that for a more accurate low-temperature behavior, Moruzzi *et al.* proposed a correction for γ based on Ref. [32], namely $\Delta\gamma = \gamma_{HT} - \gamma_{LT} = \frac{1}{3}$, which we also employ in this work. Within the Debye-Grüneisen model, the low temperature Grüneisen parameter is related to the pressure derivative of the bulk modulus $B_0' = \frac{dB}{dp}\big|_{p=0}$ via

$$\gamma_{LT}^D = \tfrac{1}{2}(B_0' - 1), \quad (2.5)$$

and can therefore be calculated directly from the EOS.

III. COMPUTATIONAL DETAILS

A. Density functional (perturbation) theory calculations

First-principles total energy calculations have been performed employing the PBEsol form of the generalized gradient approximation (GGA) [33]. The projector-augmented-wave (PAW) [34,35] method as implemented in the Vienna *ab initio* simulation package (VASP) [36,37] has been used with a plane-wave energy cutoff of 223 eV. The convergence criteria have been 10^{-6} eV for the total energy and 10^{-5} eV for the maximum energy difference in ionic relaxation steps. The integration over the Brillouin zone in the electronic structure calculations has been done using a $4 \times 4 \times 4$ and $20 \times 20 \times 20$ Monkhorst-Pack k grid [38] for the phonon supercell and the elastic primitive cell calculations, respectively. A Methfessel-Paxton [39] smearing of 0.2 eV has been used throughout the calculations. Using the k-point mesh and the energy cutoff mentioned above, the components of the elastic matrix (C_{11}, C_{12}, C_{44}) are converged within 1%.

For DFPT calculations, we use VASP in combination with PHONOPY [40]. The calculations have been done using 125-atom supercells built by a $(5 \times 5 \times 5)$ repetition of a primitive unit cell of the bcc structure. For the plots of the phonon dispersion a $(4 \times 4 \times 4)$ supercell of the conventional cell was used, which ensured to capture the features at the high symmetry points and the crossing points in the band structure more accurately. Convergence tests of the supercell size as well as the k-point mesh have been carried out resulting in an error of less than 5 meV in the vibrational free energy and a

difference in CTE smaller than $0.66 \times 10^{-6}\,\mathrm{K}^{-1}$ at the melting temperature. The integration over the phonon DOS is carried out on a q-point mesh of $100 \times 100 \times 100$.

Elastic constants are calculated using three independent distortion types (isotropic, tetragonal, and shear) as described in Ref. [41] in more detail. For each distortion type, 21 distortions in the range of $\pm 5\%$ physical strain are applied. The quality of fitting is judged using the cross validation score, which exhibited that—depending on the distortion type—the most reliable results are obtained using maximal physical strains in the range of 4%–5%, and polynomials of order 4 and 6.

B. Computation of thermal expansion coefficients

First, the internal energy contribution $U(V)$ of Eq. (2.1) is computed for 11 volumes varying from -5% to $+5\%$ with respect to the equilibrium volume. Second, the vibrational contribution to the free energy as a function of volume is calculated at a given temperature T. The considered temperature range varies from 0 to 2400 K with a step size of 10 K. Here two different models are used taking input parameters from DFT, the phonon frequencies on the one hand, and the bulk modulus and Grüneisen parameter on the other. Third, for every considered temperature the minimum of the free energy is found as a function of the volume to obtain $V_0(T)$. Finally, the CTE is obtained by numeric differentiation.

When employing the DG model, the thermodynamic Grüneisen parameter γ_{LT}^{D} is determined by a Birch Murnaghan equation of state fit of the electronic ground-state energy as a function of volume [42]. Using a parametric least squares fit of 21 energy-volume points equally distributed $\pm 15\%$ around the equilibrium volume one obtains the zero pressure values for bulk modulus B_0, its pressure derivative B_0', and the minimal energy E_0 as well as the corresponding volume V_0. The Grüneisen parameter is then obtained using Eq. (2.5).

C. Treatment of chemical disorder

To perform DFT calculations for W alloys, we use the virtual-crystal approximation (VCA). The alloy is modeled on the basis of effective atoms with intermediate nuclear and valence charge, so that the distribution of electronic charge is homogeneous in the crystal. For example, a W-50% Re alloy (all concentrations refer to at.%) is obtained with an atom of nuclear charge $Z = 74.5$ and valence charge $Z_{\mathrm{val}} = 12.5$. In this way, VCA calculations model spatially homogeneous d-band depletion or filling, depending on the alloying element.

W-Re alloys are also well suited to be studied within the VCA. Various structural and thermodynamic properties of W-Re alloys have been successfully described within the VCA [3–5]. This gives us confidence that also phonon properties of W-Re can be accurately taken into account within the VCA which allows us to compute the phonon density of states at various levels of sophistication at affordable computational cost.

IV. RESULTS

A. Elastic constants

As elastic constants provide important insights to the long wavelength limit of the phonon dispersion and serve as input for the DG model, we investigate the impact of alloying on the elastic constants. The impact of Re alloying on the lattice parameter and on the elastic constants of W is quite well established and it has been investigated both experimentally and theoretically previously [3,4,43] as summarized in Table I. The general trend is that, as a function of Re concentration, the lattice parameter decreases and the bulk modulus B increases indicative of a stiffening of the lattice with respect to hydrostatic loading. For the shear resistance, however, the picture is more complex. The concentration dependence of the bulk modulus is shown in Fig. 2 alongside with the shear

TABLE I. Lattice parameter a, bulk modulus B, shear elastic modulus G, elastic constants C', C_{11}, and C_{44}, the Grüneisen parameter γ_{HT}, and the energy difference between fcc and bcc structures $\Delta U_{\text{fcc-bcc}}$ for W and WRe alloys. Calculated lattice parameters are given in Å at $T = 0$ K. The experiment was conducted at room temperature. Elastic data are given in GPa for the respective equilibrium volumes at $T = 0$ K, energies are given in eV. Experimental elastic constants, lattice parameter, and Grüneisen parameter are taken from Refs. [44,45].

	a	B	G	C'	C_{11}	C_{12}	C_{44}	$\Delta U_{\text{fcc-bcc}}$	γ_{HT}^{D}
W (expt.)	3.165	310	161	164	532	205	162	.	1.6 (γ_{LT})
W	3.156	327	145	148	524	229	143	0.4855	1.863
WRe03	3.154	328	150	149	527	228	151	0.4692	1.873
WRe06	3.151	331	156	155	537	227	156	0.4514	1.887
WRe09	3.148	334	165	170	560	220	161	0.4321	1.906
WRe12	3.145	336	172	182	578	215	166	0.4116	1.934
WRe18	3.140	338	162	156	546	234	166	0.3682	1.995
WRe25	3.134	345	160	147	541	247	169	0.3156	2.022
WRe50	3.115	363	152	120	523	283	173	0.1161	2.039

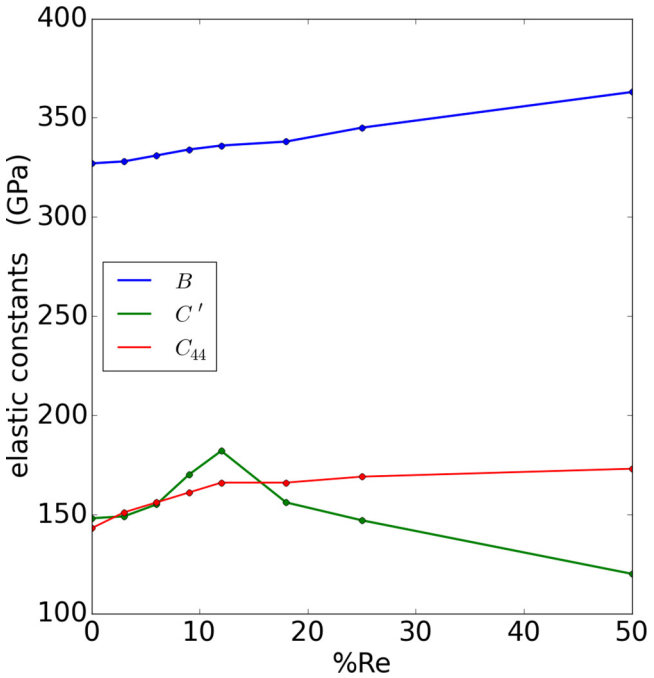

FIG. 2. Bulk modulus B and shear constants C' and C_{44} as a function of Re concentration.

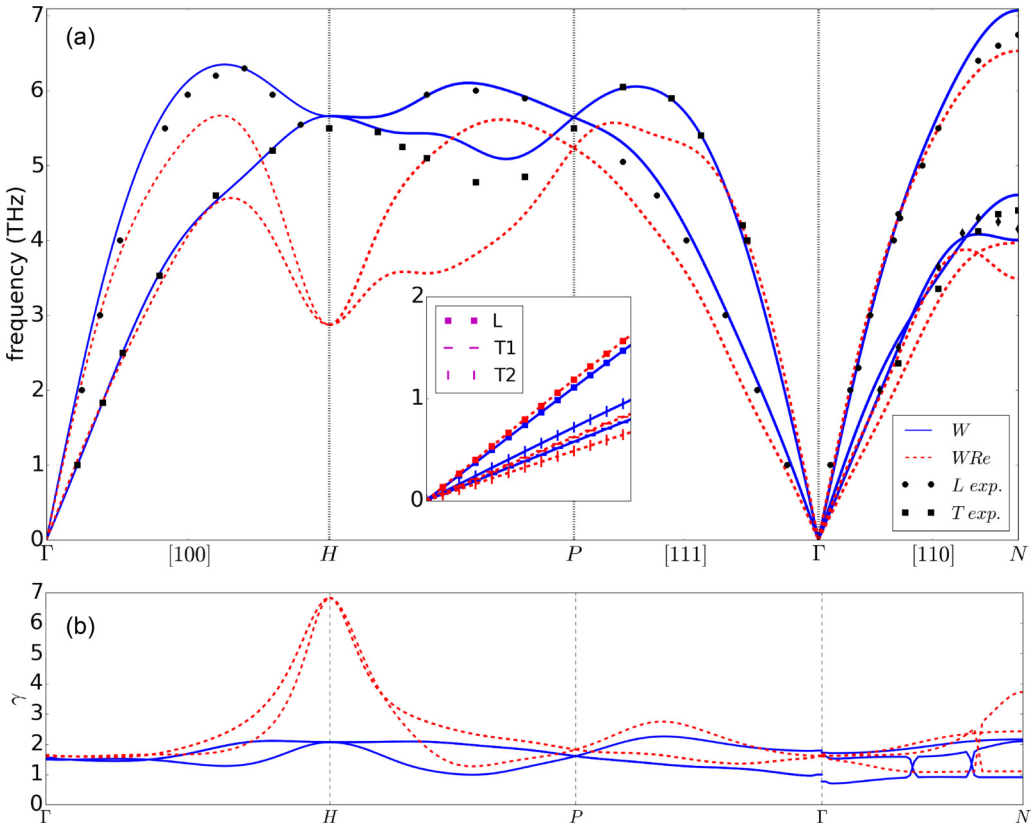

FIG. 3. (a) Phonon dispersion for pure W (solid line) and $W_{0.75}Re_{0.25}$ (dashed line) calculated at the respective theoretical equilibrium volume ($T = 300$ K). The black symbols show experimental values taken from Landolt-Börnstein [46] (measured using neutron scattering at 298 K). The inset shows the dispersion in [110] direction ($\Gamma \rightarrow N$) in more detail. (b) Mode Grüneisen parameters for W (solid line) and $W_{0.75}Re_{0.25}$ (dashed line) calculated from the logarithmic volume derivative of the respective phonon dispersion.

constants C' and C_{44}. While the shear constant C_{44} also increases monotonically with Re content, the tetragonal shear constant C' first increases up to a Re content of 12% where it has a maximum. Remarkably, at the same Re content, the dip in the CTE (compare Fig. 1) is found. For higher Re content C' experiences a softening, which has been shown to eventually lead to a negative C' for Re concentrations higher than 85 at.% [43]. On the basis of the Bain path, this softening can be correlated with a decreased energy difference between the bcc and fcc structure [43].

B. Phonons

A key to understanding the thermal expansion coefficient is to capture the essence of the phonon dispersion and the phonon density of states. In this section we will therefore compare the phononic properties obtained from density functional perturbation theory (DFPT) to those of the DG model.

Figure 3(a) shows the phonon dispersion calculated within DFPT for pristine W (blue solid lines) and $W_{0.75}Re_{0.25}$ (red dashed lines) together with results from neutron scattering experiments (black symbols). Theory and the available experiment for pure W show overall a very good agreement, both quantitatively and regarding the detailed qualitative features of the band structure. Re alloying changes the dispersion quite significantly, most prominently, regarding two important features: on the one hand, a general softening of the phonon band structure is observed, while on the other hand, the slope of certain phonon bands increases in the long wavelength limit close to the Γ point.

We first focus on the long wavelength limit. Here the slope of the phonon branches is directly connected with the elastic constants via the Christoffel equations [47] summarized in Table II for the relevant directions.

We observe the strongest influence of alloying along the [110] direction for which a closeup is shown in the inset of Fig. 3(a), where the slope of the longitudinal branch, which

TABLE II. Relation of elastic constants with the sound velocity of longitudinal and transversal branches in different high symmetry directions of the Brillouin zone.

$v_L^{[100]}$	$\sqrt{\frac{C_{11}}{\rho}}$
$v_{T1}^{[100]} = v_{T2}^{[100]}$	$\sqrt{\frac{C_{44}}{\rho}}$
$v_L^{[110]}$	$\sqrt{\frac{C_{11}+C_{12}+2C_{44}}{2\rho}}$
$v_{T1}^{[110]}$	$\sqrt{\frac{C_{44}}{\rho}}$
$v_{T2}^{[110]}$	$\sqrt{\frac{C_{11}-C_{12}}{2\rho}} = \sqrt{\frac{C'}{\rho}}$
$v_L^{[111]}$	$\sqrt{\frac{C_{11}+2C_{12}+4C_{44}}{3\rho}}$
$v_{T1}^{[111]} = v_{T2}^{[111]}$	$\sqrt{\frac{C_{11}-C_{12}+C_{44}}{3\rho}}$

is proportional to $\sqrt{C_{11}+C_{12}+2C_{44}}$, grows. This is in line with the stiffening of the bulk modulus B upon Re addition mentioned above, since $B=(C_{11}+2C_{12})/3$. Similarly, the slope of the T1 transversal branch, related to C_{44}, increases slightly. On the contrary, the slope of the second transversal branch T2, which is connected with C', decreases. All these changes upon alloying observed in the long wavelength limit of the phonon modes are in agreement with the alloying trends already noted for the elastic constants in the previous section.

Beyond the long wavelength limit, i.e., the linear dispersion regime, all phonon branches soften upon Re alloying with pronounced effects appearing near the H point and towards the P point. A similar effect has already been noted by Persson *et al.* [1] who have also observed a phonon softening in WRe alloys. However, in their work the softening is most pronounced at the $L(\frac{2}{3},\frac{2}{3},\frac{2}{3})$ point (between H and P), while no softening at the H point was observed. We found this difference to originate mainly from the choice of q-point mesh as shown in the appendix. We also note that for pure Re assuming the bcc structure, Persson *et al.* [1] have also observed a strong softening at the H point with a local maximum between Γ and H, thus showing the same trend as found in our calculations for $W_{0.75}Re_{0.25}$. Note that we have computed the phonon dispersion also for other Re concentrations, namely $W_{0.97}Re_{0.03}$, $W_{0.94}Re_{0.06}$, $W_{0.91}Re_{0.09}$, $W_{0.88}Re_{0.12}$, $W_{0.82}Re_{0.18}$, $W_{0.75}Re_{0.25}$, and $W_{0.50}Re_{0.50}$, where we consistently find a gradual softening of the high-k modes as discussed above. Only for concentrations above $W_{0.75}Re_{0.25}$ the softening at $L(\frac{2}{3},\frac{2}{3},\frac{2}{3})$ gets gradually more pronounced and finally shows an instability for pure bcc Re.

In addition to the phonon dispersion, another quantity directly related to the CTE is the Grüneisen parameter. The thermodynamic definition of the Grüneisen parameter traditionally obtained from the equation of state via Eq. (2.5) is given in Table I. We notice a monotonous increase upon Re% addition. Therefore, this is not able to explain the stiffening related to the anomaly in the CTE. Furthermore, a relative increase of γ^D_{HT} of only 0.175 when comparing pure W and WRe50 is not able to describe the increase in CTE as this is counteracted by a strong decrease in the equilibrium volume. Therefore we calculated the mode Grüneisen parameters directly from the logarithmic volume derivative of the phonon dispersion.

Figure 3(b) shows the mode Grüneisen parameters obtained from the logarithmic volume derivative of the phonon dispersion curves. Also here we notice a significant increase for $W_{0.75}Re_{0.25}$ especially at the H point. In order to be able to draw conclusions on the CTE the quantity of choice is the averaged Grüneisen parameter. It is directly related to the CTE by [48]

$$\alpha \sim \frac{\bar{\gamma}_{HT}}{BV}. \tag{4.1}$$

The averaged mode Grüneisen parameter is shown in Fig. 4. Here we can see a pronounced stiffening around 10% Re which is already an indication that the anomaly in CTE can be described by the explicit phonon calculations. Furthermore, the overall increase when going to higher Re content is much more pronounced as in the Grüneisen γ^D_{HT} obtained from the EOS.

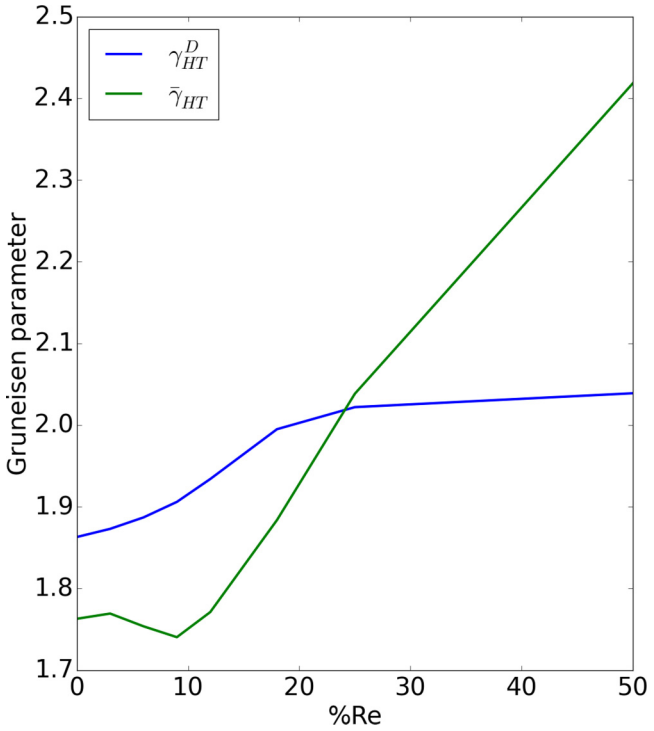

FIG. 4. Grüneisen parameters $\bar{\gamma}_{HT}$ and γ^D_{HT} as a function of Re content.

To narrow down the origin of the nonmonotonous behavior of the Grüneisen parameter upon Re addition, we choose a different representation. In Fig. 5 we show the mode Grüneisen parameter averaged over spherical shells $|q+\delta q|$ as a function of q. With this representation we are able to investigate the behavior of γ with Re addition with respect to the magnitude of the q vector. The most interesting features are the sudden decrease of γ in the long wavelength limit for concentrations between 6% and 9% Re and the strong increase for larger $|q|$ for concentrations >12% Re.

The impact of Re alloying is also nicely seen in the phonon density of states (DOS) shown in the bottom panel of Fig. 6. Here the shaded areas correspond to the phonon DOS obtained from DFPT for pristine W (blue) and for $W_{0.75}Re_{0.25}$ (red). Again, the main overall effect upon Re addition is to lower the phonon frequencies as can be clearly seen by the shift towards lower frequencies for the two main peaks of the DOS, denoted as M_{trans} and M_{long} for transversal and longitudinal phonons, respectively. This shift as a function of Re concentration occurs monotonically and more strongly for the transversal branch than for the longitudinal branch. Only for small phonon frequencies corresponding to the limit of very long wavelengths where the phonon DOS is parabolic, the effect is reversed as can be seen from the inset. Here pure W has a slightly larger DOS than $W_{0.75}Re_{0.25}$ (see inset Fig. 6). However, the relative weight of this region in the integration carried out to obtain the vibrational free energy from Eq. (2.2) is small.

We now compare the *ab initio* phonon DOS obtained within DFPT with the corresponding DOS from the Debye model shown in the top panel of Fig. 6 for W and $W_{0.75}Re_{0.25}$. In the long wavelength (low frequency) limit, the shape of

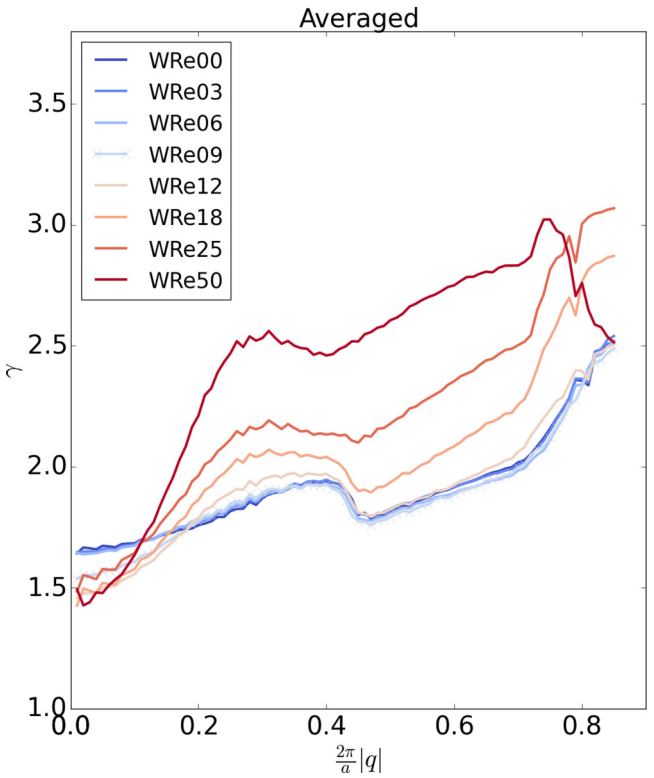

FIG. 5. Averaged mode Grüneisen parameters γ for WRe as a function of the norm of the q vector. The averaged Grüneisen parameter is plotted for pure W (dark blue) and for WRe with Re contents ranging up to 50% (dark red).

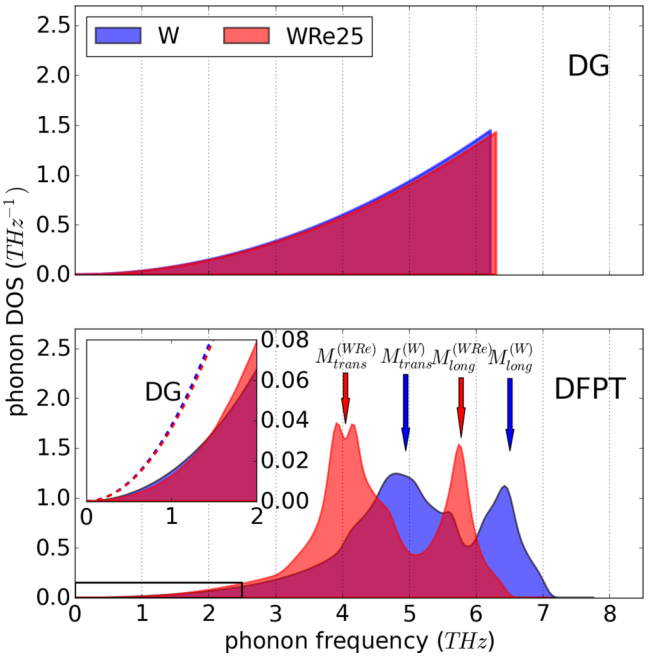

FIG. 6. Phonon density of states (DOS) for W (blue) and WRe25 (red) obtained from different approaches: The upper panel shows the DOS obtained using the DG model, and the lower panel the one obtained from DFPT calculations, respectively. In the bottom panel the labels M_{trans} and M_{long} indicate the maxima of the phonon DOS for longitudinal and transversal phonons, respectively. A detail for small wave vectors of the Debye-Grüneisen model (dashed lines) compared to the phonon DOS obtained from DFPT (colored faces) is shown in the inset. All DOS are calculated for the equilibrium lattice parameter at $T = 0$ K.

the Debye model is in qualitative agreement with the DFPT results. As expected, beyond this limit the DOS is considerably different. The success of the Debye model for many systems relies on the fact that the vibrational free energy results from an integration over the entire frequency axis. As a consequence, integrated properties are often not so sensitive to the exact structure of the DOS. However, at this point we can already expect a shortcoming of the DG model when applied to WRe alloys since it fails to capture the correct softening at high frequencies. As can be seen in Fig. 6, the Debye frequency ω_D *increases* with Re alloying, while an overall phonon softening upon Re alloying is found in the DFPT calculation.

C. Thermal expansion

1. Debye-Grüneisen model (DG)

First, we address whether the evolution of the CTE with alloying content can be reproduced using the DG model which is computationally much less demanding. As shown earlier in Fig. 2 and Table I, Re alloying increases both B and γ_{HT}^{D}. The two major driving forces for changing the CTE, hence, counteract each other. The resulting CTE is shown in Fig. 7 with solid lines. When comparing the concentration dependence of the CTE at fixed temperature, the agreement with experiment is quite poor. The absolute values are considerably overestimated (about 20% for low Re concentrations), and, more importantly, the CTE increases only slightly with Re alloying below 20% and even decreases

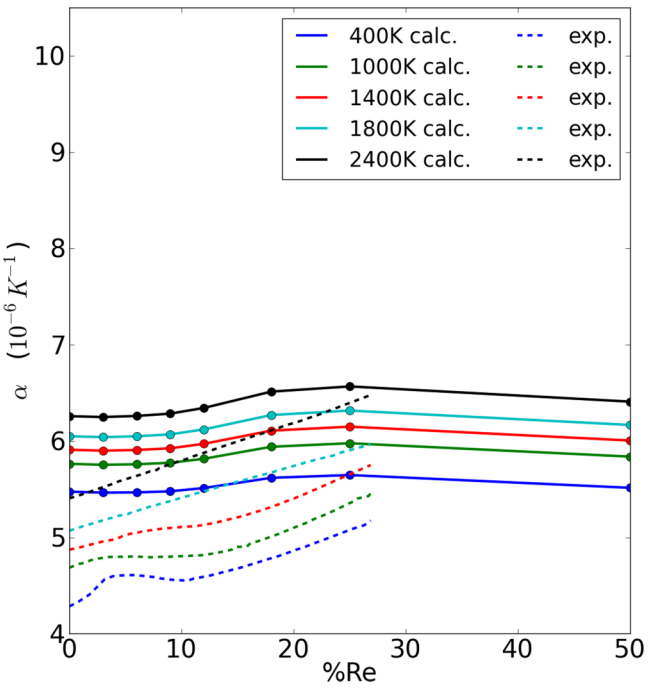

FIG. 7. Thermal expansion coefficients of WRe alloys as a function of the Re concentration for various temperatures. Dashed lines are fits to the experimental data points from Ref. [7], while the solid lines depict our results using the Debye-Grüneisen model.

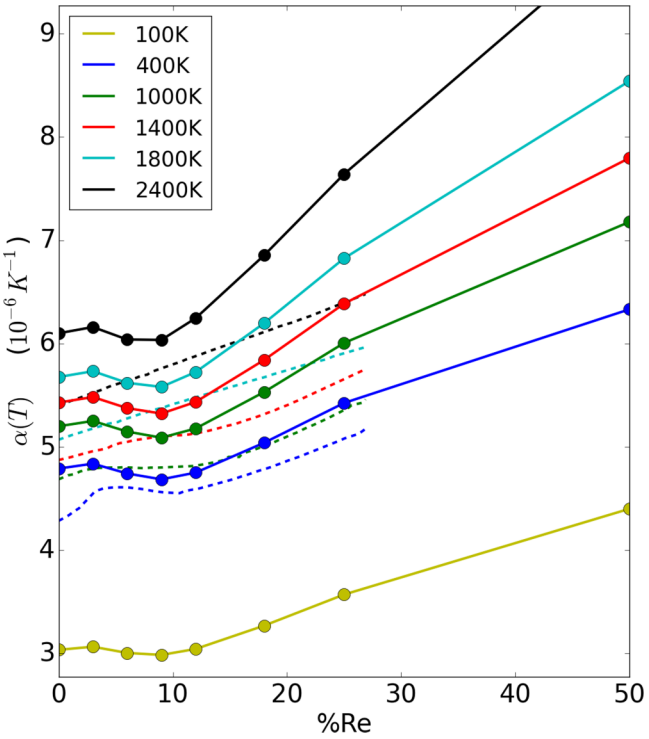

FIG. 8. Isotherms of the thermal expansion coefficient with respect to Re content. Dashed lines are experimental measurements [7]. Solid lines correspond to our results based on the *ab initio* phonon DOS from density functional perturbation theory.

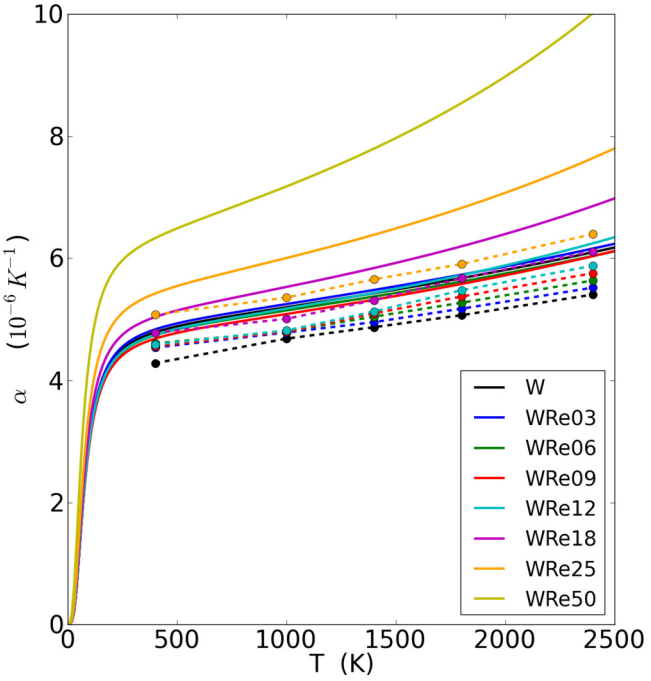

FIG. 9. Thermal expansion coefficients of WRe alloys at different Re concentrations as a function of the temperature calculated in the QHA with explicit phonon calculations. Dashed lines show experimental values from Ref. [7], where the colors correspond to the same Re concentrations as in the theoretical results.

when going up to 50% Re content. We conclude that the DG model fails to reproduce alloying trends correctly in the WRe system. Thus, the assumption that the CTE in this material can be derived from the equation of state only, appears to be too drastic. The DG model misses both, the softening in shear and the softening of phonon modes.

2. *Ab initio phonon dispersion*

In order to obtain the CTE from a more reliable description of the vibrational free energy, we use explicit *ab initio* phonon spectrum calculations by means of density functional perturbation theory. As described in Sec. II, the phonon spectrum is a decisive parameter that determines the accuracy of the phonon free energy and, subsequently, of the CTE.

Figure 8 shows the thermal expansion coefficients of W and WRe calculated in the QHA using DFPT in comparison with experimental results [7]. The theoretical curves show a nonmonotonous progression with alloying at all temperatures (Fig. 8): Small Re additions induce a reduction of the CTE followed by an increase for Re concentrations larger than 12%. This is in good agreement with experiment, which equivalently shows a local minimum of the CTE around 12% Re content for temperatures up to 1000 K. Only for higher temperatures this anomaly disappears in the experiment. Thus, for temperatures up to 1000 K the DFPT calculations reproduce both, the increase in CTE for large Re concentration as well as the anomalous behavior of the CTE at low concentrations. For temperatures above 1000 K, higher order anharmonic effects come into play [24,45]. Therefore, further investigations including explicit anharmonicity become necessary to reproduce the disappearance of the anomaly.

For the sake of completeness, in Fig. 9 we also show the CTE as a function of *temperature* for all calculated alloy compositions including experimental values.

V. CONCLUSION

We have investigated the alloying effect of Re on the elastic properties, phonons, and thermal expansion of W. We have found that Re addition affects different elastic constants in a different way, i.e., B and C_{44} are increasing, while C' shows a nonmonotonous behavior with a maximum at 12%. We have analyzed the effect of Re on the phonon dispersion and have found that Re generally reduces the vibrational frequencies, while only the longitudinal modes close to the Γ point are slightly increased. Regarding the thermal expansion coefficient of WRe, we have used two approaches with different complexity, namely the traditional DG model [11] and the QHA including explicit linear-response phonon calculations. We have investigated the atypical concentration dependence of the thermal expansion coefficient observed in experiment, showing a decrease for low Re content (9%) but an increase for higher concentrations. We have shown that the anomalous decrease for low Re content originates from a decrease of the averaged Grüneisen parameter for long wavelength phonons. For the same Re content C' shows a maximum. The increase

of the CTE for higher Re contents originates from a strong phonon softening at smaller wavelengths accompanied by an increase of the Grüneisen parameter.

The Debye-Grüneisen model fails for two reasons. First, elastic anisotropy is not taken into account and second, the thermodynamic Grüneisen parameter determined by the equation of state neither shows a decrease for low Re content nor does it show an increase for higher Re contents strong enough to counteract the isotropic stiffening.

We conclude that in order to describe the thermal expansion of WRe appropriately, explicit phonon calculations are needed which take into account both the phonon softening beyond the long wavelength limit and the anisotropic behavior of the phonon branches close the the Γ point. To account for the disappearance of the anomaly observed in experiment above 1000 K further investigation is necessary also accounting for higher order anharmonic effects.

ACKNOWLEDGMENTS

Financial support by the Austrian Federal Government (in particular from Bundesministerium für Verkehr, Innovation und Technologie and Bundesministerium für Wissenschaft, Forschung und Wirtschaft) represented by Österreichische Forschungsförderungsgesellschaft mbH and the Styrian and the Tyrolean Provincial Government, represented by Steirische Wirtschaftsförderungsgesellschaft mbH and Standortagentur Tirol, within the framework of the COMET Funding Programme are gratefully acknowledged.

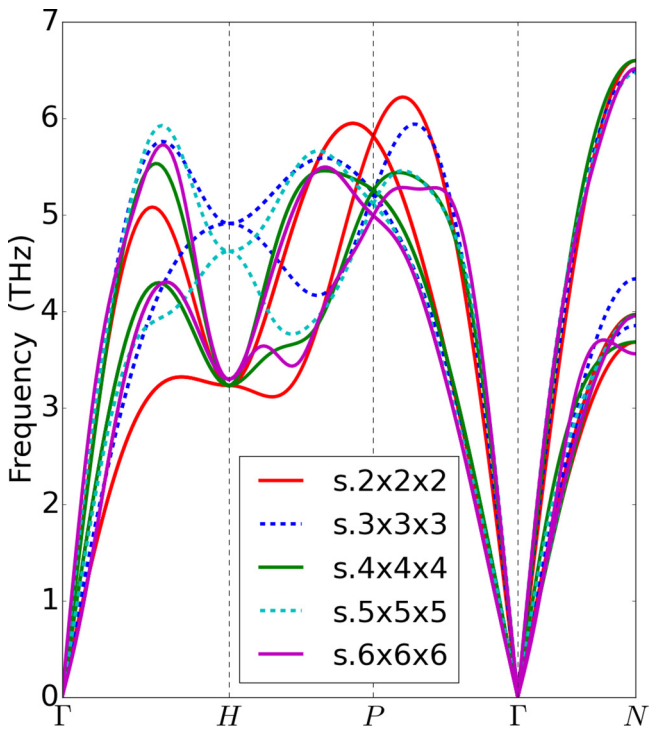

FIG. 10. Phonon dispersion of WRe25 shown for different supercells of the primitive cell. Dashed lines indicate supercells constructed with an odd number of primitive cells in each direction and solid lines such with an even number of primitive cells.

TABLE III. Comparison of computational methods and parameters used for calculating the phonon dispersion of W and WRe by Persson *et al.* [1] and in our work.

	This work	Ref. [1]
Reference cell	conventional cell	primitive cell
Supercell size or q-mesh	$4 \times 4 \times 4$	$5 \times 5 \times 5$
k-point mesh for electronic structure	$5 \times 5 \times 5$ Monkhorst-Pack (equiv. to $20 \times 20 \times 20$)	$16 \times 16 \times 16$ Monkhorst-Pack
Method to calculate phonons	Gamma point DFPT + supercell method	DFPT

APPENDIX: PHONON DISPERSION OF WRE: CHOICE OF q-POINT MESH

The importance of the choice of q mesh for obtaining a good phonon dispersion of $W_{0.75}Re_{0.25}$ becomes clear when looking at the convergence with respect to the supercell size. Figure 10 shows the results for different supercells sizes $n \times n \times n$ for supercells constructed from the primitive cell (P-SC). Note that an $n \times n \times n$ P-SC is equivalent to an $n \times n \times n$ q-point mesh for a primitive cell and the comparison of the two methods used

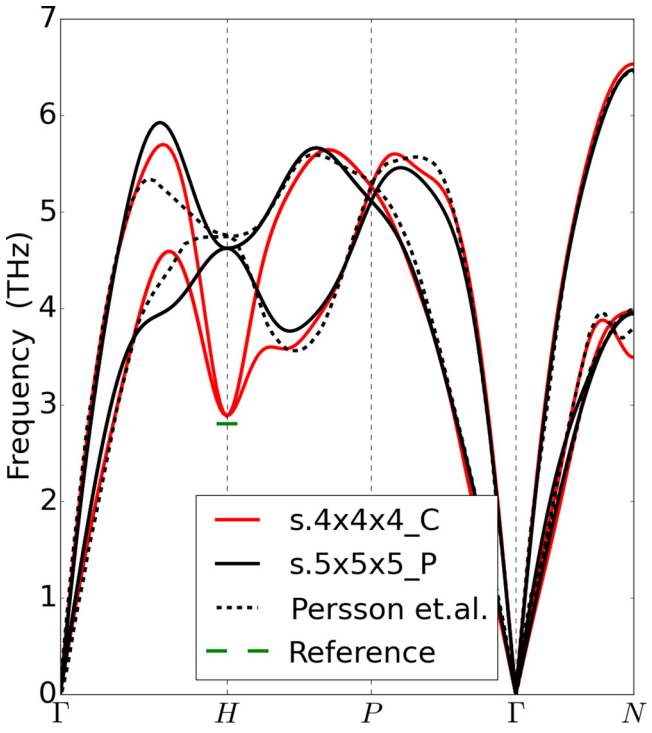

FIG. 11. Comparison of phonon dispersions of WRe25 calculated using different supercells with the phonon dispersion published by Persson *et al.*: Solid red lines represent the results for a $4 \times 4 \times 4$ supercell of the conventional cell (C-SC), solid black lines represents our calculation using a $5 \times 5 \times 5$ supercell of the primitive cell (P-SC) and the dashed line the results of Persson *et al.* The green marker indicates the position of the fully converged frequency at the H point which is considered as reference here.

by Persson *et al.* and in our work is therefore straight forward (see Table III). At the H point the influence of the mesh on the convergence is specially pronounced: While even the smallest *even* meshes (or supercell sizes) capture this point very well, odd meshes converge extremely slowly. We confirmed this also using a different VSC potential with QUANTUM ESPRESSO [49]. The distinct convergence behavior of odd and even meshes at the H point is due to the fact that this point, which has reciprocal primitive coordinates $(\frac{1}{2},\frac{1}{2},\frac{1}{2})$, is explicitly contained in *any even mesh*, while it is not there in odd ones.

To get reliable reference values for the frequencies at the H point, also convergence studies with respect to the k mesh used for the electronic structure calculations were carried out. To do so we used the $2 \times 2 \times 2$ P-SC, which is the smallest supercell containing the H point explicitly. Convergence for the H point was reached for a $24 \times 24 \times 24$ k mesh within 0.1 THz, giving a frequency at the H point of 2.75 THz. The main results are given in Fig. 11. If using a $5 \times 5 \times 5$ P-SC we get similar results as Persson *et al.* who used a $5 \times 5 \times 5$ q-point mesh but are far from the converged reference frequency at the H point. The $4 \times 4 \times 4$ C-SC used in this work, in contrast, contains the H point explicitly and naturally describes its phonon eigenvalues, as well as the features of other high-symmetry points, very well.

[1] K. Persson, M. Ekman, and G. Grimvall, Phys. Rev. B **60**, 9999 (1999).
[2] M. Ekman, K. Persson, and G. Grimvall, J. Nucl. Mater. **278**, 273 (2000).
[3] L. Romaner, C. Ambrosch-Draxl, and R. Pippan, Phys. Rev. Lett. **104**, 195503 (2010).
[4] H. Li, S. Wurster, C. Motz, L. Romaner, C. Ambrosch-Draxl, and R. Pippan, Acta Mater. **60**, 748 (2012).
[5] D. Scheiber, V. I. Razumovskiy, P. Puschnig, R. Pippan, and L. Romaner, Acta Mater. **88**, 180 (2015).
[6] Plansee SE, Material Data Base, Reutte, Austria, 2000.
[7] V. G. Andrianova, A. Z. Zhunk, V. M. Zaichenko, E. B. Zaretskii, V. A. Petukhov, and V. Ya. Chekhovskoi, Teplofiz. Vys. Temp. **21**, 80 (1983) [High Temp. **21**, 70 (1983)].
[8] V. M. Zaichenko, R. G. Mints, V. A. Petukhov, and V. Ya. Chekhovskoi, Teplofiz. Vys. Temp. **12**, 1015 (1974) [High Temp. **12**, 889 (1974)].
[9] R. A. Ayres, G. Shanette, and D. Stein, J. Appl. Phys. **46**, 1526 (1975).
[10] M. Chakraborty, J. Spitaler, P. Puschnig, and C. Ambrosch-Draxl, Comput. Phys. Commun. **181**, 913 (2010).
[11] V. L. Moruzzi, J. F. Janak, and K. Schwarz, Phys. Rev. B **37**, 790 (1988).
[12] G. Grimvall, *Thermophysical Properties of Materials* (Elsevier Science, Amsterdam, 1999).
[13] S. Feng, S. Li, and H. Fu, Comput. Mater. Sci. **82**, 45 (2014).
[14] Y.-D. Guo, X.-S. Song, X.-B. Li, and X.-D. Yang, Solid State Commun. **141**, 577 (2007).
[15] H. M. Jin and P. Wu, J. Alloys Compd. **343**, 71 (2002).
[16] Y. Liang, S. Shang, J. Wang, Y. Wang, F. Ye, J. Lin, G. Chen, and Z. Liu, Intermetallics **19**, 1374 (2011).
[17] X.-K. Liu, W. Zhou, Z. Zheng, and S.-M. Peng, J. Alloys Compd. **615**, 975 (2014).
[18] B. Mayer, H. Anton, E. Bott, M. Methfessel, J. Sticht, J. Harris, and P. Schmidt, Intermetallics **11**, 23 (2003).
[19] J. Ning, X. Zhang, X. Huang, N. Sun, M. Ma, and R. Liu, Intermetallics **54**, 7 (2014).
[20] S.-L. Shang, Y. Wang, D. Kim, and Z.-K. Liu, Comput. Mater. Sci. **47**, 1040 (2010).
[21] C. Toher, J. J. Plata, O. Levy, M. de Jong, M. Asta, M. B. Nardelli, and S. Curtarolo, Phys. Rev. B **90**, 174107 (2014).
[22] W. Xu, J. Han, Z. Wang, C. Wang, Y. Wen, X. Liua, and Z. Zhu, Intermetallics **32**, 303 (2013).
[23] Z.-Y. Zeng, C.-E. Hu, L.-C. Cai, X.-R. Chen, and F.-Q. Jing, Phys. B-Condens. Matter **405**, 3665 (2010).
[24] G. J. Ackland, X. Huang, and K. M. Rabe, Phys. Rev. B **68**, 214104 (2003).
[25] M. E. Williams, Master's thesis, Texas A&M University, 2008.
[26] F. Han, *A Modern Course in the Quantum Theory of Solids* (World Scientific Pub Co Inc., Singapore, 2012).
[27] S. Baroni, P. Giannozzi, and A. Testa, Phys. Rev. Lett. **58**, 1861 (1987).
[28] X. Gonze and C. Lee, Phys. Rev. B **55**, 10355 (1997).
[29] S. Baroni, S. de Gironcoli, A. D. Corso, and P. Giannozzi, Rev. Mod. Phys. **73**, 515 (2001).
[30] P. A. Korzhavyi, A. V. Ruban, S. I. Simak, and Y. K. Vekilov, Phys. Rev. B **49**, 14229 (1994).
[31] O. Anderson, in *Lattice Dynamics*, Physical Acoustics, Vol. 3, Part B, edited by W. P. Mason (Academic, New York, 1965), pp. 43–95.
[32] T. Barron, Philos. Mag. **46**, 720 (1955).
[33] J. P. Perdew, A. Ruzsinszky, G. I. Csonka, O. A. Vydrov, G. E. Scuseria, L. A. Constantin, X. Zhou, and K. Burke, Phys. Rev. Lett. **100**, 136406 (2008).
[34] P. E. Blöchl, Phys. Rev. B **50**, 17953 (1994).
[35] G. Kresse and D. Joubert, Phys. Rev. B **59**, 1758 (1999).
[36] G. Kresse and J. Furthmuller, Comput. Mat. Sci. **6**, 15 (1996).
[37] G. Kresse and J. Furthmuller, Phys. Rev. B **54**, 11169 (1996).
[38] H. J. Monkhorst and J. D. Pack, Phys. Rev. B **13**, 5188 (1976).
[39] M. Methfessel and A. T. Paxton, Phys. Rev. B **40**, 3616 (1989).
[40] A. Togo, F. Oba, and I. Tanaka, Phys. Rev. B **78**, 134106 (2008).
[41] R. Golesorkhtabar, P. Pavone, J. Spitaler, P. Puschnig, and C. Draxl, Comput. Phys. Commun. **184**, 1861 (2013).
[42] F. Birch, Phys. Rev. **71**, 809 (1947).
[43] P. Souvatzis, M. I. Katsnelson, S. I. Simak, R. Ahuja, O. Eriksson, and P. Mohn, Phys. Rev. B **70**, 012201 (2004).
[44] G. Simmons and H. Wang, *Single Crystal Elastic Constants and Calculated Aggregate Properties: A Handbook* (MIT Press, Cambridge, 1971).
[45] A. F. Guillermet and G. Grimvall, Phys. Rev. B **44**, 4332 (1991).
[46] H. R. Schober and P. H. Dederichs, *in Phonon States of Elements. Electron States and Fermi Surfaces of Alloys*, edited by K.-H. Hellwege and J. L. Olsen, Landolt-Börnstein–Group III Condensed Matter (Springer-Verlag, Berlin, Heidelberg, 1981), Vol. 13A.

[47] V. Vavryčuk, Proc. R. Soc. London Ser. A **462**, 883 (2006).
[48] P. Nath, J. J. Plata, D. Usanmaz, R. A. R. A. Orabi, M. Fornari, M. B. Nardelli, C. Toher, and S. Curtarolo, Comput. Mater. Sci. **125**, 82 (2016).
[49] P. Giannozzi, S. Baroni, N. Bonini, M. Calandra, R. Car, C. Cavazzoni, D. Ceresoli, G. L. Chiarotti, M. Cococcioni, I. Dabo, A. D. Corso, S. de Gironcoli, S. Fabris, G. Fratesi, R. Gebauer, U. Gerstmann, C. Gougoussis, A. Kokalj, M. Lazzeri, L. Martin-Samos, N. Marzari, F. Mauri, R. Mazzarello, S. Paolini, A. Pasquarello, L. Paulatto, C. Sbraccia, S. Scandolo, G. Sclauzero, A. P. Seitsonen, A. Smogunov, P. Umari, and R. M. Wentzcovitch, J. Phys.: Condens. Matter **21**, 395502 (2009).